Cold Regions Science and Technology 212 (2023) 103881

Contents lists available at ScienceDirect

Cold Regions Science and Technology

journal homepage: www.elsevier.com/locate/coldregions

Simulating the thermal regime of a railway embankment structure on the Tibetan Plateau under climate change

Rui Chen [a,b,*], Thomas Schneider von Deimling [a,b], Julia Boike [a,b], Qingbai Wu [c], Moritz Langer [a,d]

[a] Permafrost Research Section, Alfred Wegener Institute Helmholtz Centre for Polar and Marine Research, Potsdam 14473, Germany
[b] Geography Department, Humboldt-Universität zu Berlin, Berlin 10099, Germany
[c] State Key Laboratory of Frozen Soil Engineering, Northwest Institute of Eco-Environment and Resources, Chinese Academy of Sciences, Lanzhou 730000, China
[d] Department of Earth Sciences, Vrije Universiteit Amsterdam, Amsterdam 1081 HV, The Netherlands

ARTICLE INFO

Keywords:
Infrastructure stability
Permafrost degradation
Climate change
Qinghai-Tibet Railway

ABSTRACT

With global warming and its amplified effect on the Tibetan Plateau, the permafrost on the Tibetan Plateau has been significantly degraded, manifested by decreased permafrost thickness, increased active layer thickness, thermokarst, and surface subsidence, causing severe damage to infrastructure. To better understand and assess the future stability of the Qinghai-Tibet Railway, we used a laterally coupled version of the one-dimensional CryoGrid3 land surface model to simulate the thermal regimes of the railway subgrade under current climate conditions. By modeling ground subsidence (i.e., by simulating the melting of excess ice) we provide estimates of future subgrade stability under low (Representative Concentration Pathway 2.6 [RCP2.6]) and high (RCP8.5) climate warming scenarios. Our modeled results reveal satisfactory performance with respect to the comparison of measured and modeled ground thermal regimes. Under current climate conditions, we infer that mostly thaw-stable conditions as maximum thaw depths do not reach the embankment base. The sunny side of the embankment (southeast-facing) reveals being more vulnerable to suffering from thaw settlement or thermal erosion than the shady side (northwest-facing). The extent of future railway failure due to thawing permafrost will depend on the magnitude of the warming. For conditions typical of Beiluhe (situated on continuous permafrost in the central Tibetan Plateau), the railway embankment might largely maintain safe operation until the end of the century under a scenario of climate stabilization. In contrast, under strong warming the railway subgrade is likely to destabilize from the 2030s onwards and embankment subsidence is initiated at mid-century through the melting of excess ice.

1. Introduction

The Tibetan Plateau (TP) covers an area of approximately 2.5×10^6 km^2 with a mean elevation of 4000 m above sea level. Approximately 1.15×10^6 km^2 of the TP is underlain by permafrost (Ran et al., 2021). Previous studies showed that the TP has been experiencing a strong warming trend of 0.42–0.46 °C/decade since the 1980s (Duan and Xiao, 2015; Wang et al., 2017; Yan et al., 2020), and it is estimated that the mean annual surface air temperature (MAAT) of the TP will rise by 1.9 °C (Shared Socioeconomic Pathway [SSP1–2.6]) to 6.3 °C (SSP5–8.5) by the end of the 21st century compared to 1981–2010 (Chen et al., 2022). Permafrost degradation has been widespread on the TP due to past climate warming and increasing human activity (Yang et al., 2019; Wang et al., 2022). Moreover, it is estimated that the permafrost area over the TP will shrink by 26.9% to 80.1% by the end of this century under the SSP1–2.6 to SSP5–8.5 scenarios, respectively, compared to the current permafrost extent (2001–2018) (Yin et al., 2021). Average active layer thickness (ALT) is expected to increase by 2.5 cm/decade to 17.5 cm/decade (Xu and Wu, 2021). The integrity of many human constructions on the TP has been threatened by the rapid melting of the permafrost (Wu et al., 2020a). For example, the long-term monitoring data of the Qinghai-Tibet Highway indicate thaw settlement is occurring at all sites (2004–2012), with settlement rate thresholds ranging from 1.1 cm/year to 3.1 cm/year (Peng et al., 2015), and road safety is also affected by talik development beneath embankments (Wu et al., 2002). Thaw settlement is also the principal cause for the

* Corresponding author at: Permafrost Research Section, Alfred Wegener Institute Helmholtz Centre for Polar and Marine Research, Potsdam 14473, Germany.
E-mail address: rui.chen@awi.de (R. Chen).

https://doi.org/10.1016/j.coldregions.2023.103881
Received 30 March 2022; Received in revised form 21 April 2023; Accepted 4 May 2023
Available online 5 May 2023

deformation of transmission towers, which have settled as much as 110 mm from 2011 to 2014 (Guo et al., 2016).

Approximately 50% of the Qinghai-Tibet Railway (QTR) is built on top of permafrost (Yang et al., 2018). Field investigations have observed excessive thaw settlement, longitudinal cracking, and uneven deformation, which seriously threaten the long-term safe operation of the QTR (Ma et al., 2008, 2012; Qin et al., 2010; Wu et al., 2014). Therefore, to maintain the long-term structural integrity of the railway embankment, a variety of geotechnical methods have been proposed to reinforce the railway, such as crushed rock embankments, ventilation ducts, and thermosyphons, to adjust and control the thermal state of the underlying permafrost (Cheng et al., 2008). Approximately 60% of the railway (Ma et al., 2008) that passes through the permafrost region uses a crushed-rock structure embankment (Wu et al., 2020b) due to the construction costs and the convenience of construction operation. Studies using monitoring data indicated that a crushed-rock embankment structure is able to protect the permafrost beneath the railway against warming better than the traditional embankment, with the degree of protection depending on the specific embankment structure (Niu et al., 2015; Zhao et al., 2019; Tai et al., 2020a). Therefore, reinforcing engineering techniques must be implemented to ensure the safe operation of the QTR and to adapt to rising temperatures in the future (Mu et al., 2010; Wu et al., 2020b).

To efficiently guide and maintain future foundation engineering atop permafrost, numerical modeling is a potent tool for analyzing the thermal state of crushed-rock embankments and assessing the long-term thermal stability of its subgrade (Fortier et al., 2011; Hjort et al., 2022; Kong et al., 2019; Tian et al., 2019). Lai (2003), Lai et al., 2004a, 2004b, 2006) carried out the first thermal modeling of ripped-rock embankments along the QTR using a finite-element method and indicated that such embankments can protect infrastructure under climate warming. Subsequently, utilizing the modeling method from Lai (2003), further studies explored the thermal regime dynamics at the QTR for different types of crushed-rock embankments under climate warming (Zhang et al., 2005; Li et al., 2009; Yu et al., 2016; Chen et al., 2018; Tai et al., 2020b). Additionally, sensitivity analyses of crushed rock embankment design parameters (such as height of ballast layer, slope angle, crushed-rock particle size, and thickness of the crushed-rock revetment) have illustrated its large impact on the ground thermal state (Sun et al., 2005, 2009; Zhang et al., 2007, 2009). The models used in these studies also allow for resolving construction details with high spatial resolution and show great simulation performance under current climate conditions, but they are not designed to investigate long-term climate change impacts. For example, for describing changes in the upper boundary condition through climate warming, the MAAT is assumed to linearly rise in the future. By forcing our model with dynamical upper surface boundary conditions, we account for the dynamical long-term evolution of climate parameters which impacts on the thermal regime of the railway embankment. By explicitly modeling ground subsidence (which is in general not simulated by most state-of-the-art models) we have a tool that allows us to analyze infrastructure failure as a consequence of excess ice melt. We take advantage of a two-year observed ground temperature dataset (01-01-2015 to 31-12-2016) recorded at different locations of the railway embankment (for detailed information see Supplementary Data Text S1) to validate the model by comparing field measurements with simulation results. The main objectives of this study are:

1. to demonstrate the capacity of CryoGrid3 for modeling the thermal regime of a railway embankment on the TP for present-day conditions.
2. to explore the degree to which the embankment subgrade is subject to thaw under a low (RCP2.6) and high (RCP8.5) emission scenario.
3. to discuss the potential risk and timing of the QTR failure in the future as a consequence of ground subsidence due to melting of excess ice.

2. Methods

2.1. Study site

The total length of the QTR from Golmud to Lhasa is about 1142 km, of which 550 km is underlain by permafrost. Our study site (34.8082°N, 92.9155°E, 4628 m above sea level) is in the Beiluhe Basin which is a typical continuous permafrost area in the central TP (Fig. 1). The study area is on top of upland plain landforms formed by fluvial and deluvial sediments. The surface sediments are dominated by fine to gravelly sands and stones (Yin et al., 2017; Yi et al., 2018). The vegetation type is mainly alpine meadow (Wu et al., 2016). A weather station was set up in 2002 to record meteorological variables. The mean annual air temperature, mean summer (June to August) air temperature, and mean winter (December to February) air temperature were − 3.61 °C, 5.27 °C, and − 12.44 °C, respectively, while the mean annual precipitation, mean summer precipitation, and mean winter precipitation were 365.7 mm, 248.3 mm, and 5.3 mm, respectively (Yi et al., 2018). Although most of the precipitation (over 90%) occurs from May to September in the form of rain (Yin et al., 2017), 10% of annual precipitation falls as snow (You et al., 2017). Field results indicated that mean annual ground temperatures at the top of the permafrost range from −1.5 to 0 °C and active layer thicknesses ranged from 1.4 to 3.4 m in the study area (Yin et al., 2017). The ice content and soil moisture of the permafrost in the Beiluhe Basin depend on soil characteristics and vegetation types (Yin et al., 2017). Borehole data show the depth of zero annual amplitude at about 6.2 m and the lower permafrost boundary at about 20 m (Yi et al., 2018).

2.2. Model description

To simulate the impact of permafrost degradation on the QTR embankment under climate change, we used a laterally coupled tailored version of the one-dimensional CryoGrid3 land surface model, which was originally applied for the simulation of soil thermal regimes, ground subsidence, and thermokarst in the Arctic (Langer et al., 2016; Westermann et al., 2016). The model includes an explicit surface energy balance scheme, a subsurface heat conduction scheme, a dynamic snowpack scheme, a water infiltration scheme, and an excess ground-ice melt scheme (Westermann et al., 2016, see also Supplementary Data Text S2 for more details). The surface energy module describes an upper model boundary condition that calculates the energy fluxes at the ground surface (Westermann et al., 2016), accounting for the exchange of latent and sensible heat (Nitzbon et al., 2019, 2020, 2021; Martin et al., 2021). The CryoGrid3 model has been used in previous studies to investigate landscape dynamics and processes aspects such as e.g., the heat transfer between water bodies and permafrost (Langer et al., 2016), polygonal tundra dynamics (Nitzbon et al., 2019, 2020, 2021), permafrost-forest interactions (Stuenzi et al., 2021), and the degradation of permafrost under a gravel road (Schneider von Deimling et al., 2021).

For this study, we use a model version with a lateral exchange of heat and water between adjacent tiles (Nitzbon et al., 2019), and activated ground subsidence scheme based on excess ice melting (Nitzbon et al., 2021). We mainly build on a model setup developed for simulating linear infrastructure constructed on top of permafrost (Schneider von Deimling et al., 2021). Table 1 summarizes specific parameter settings used in this study, while all remaining model parameters (see Supplementary Data Table S1) were set to default values as defined by Westermann et al. (2016) and Nitzbon et al. (2019). Supplementary Data Text S2 describes in more detail the model structure and key individual model schemes.

2.3. Model setup

2.3.1. Embankment structure

The railway section at our Beiluhe study site is characterized by a

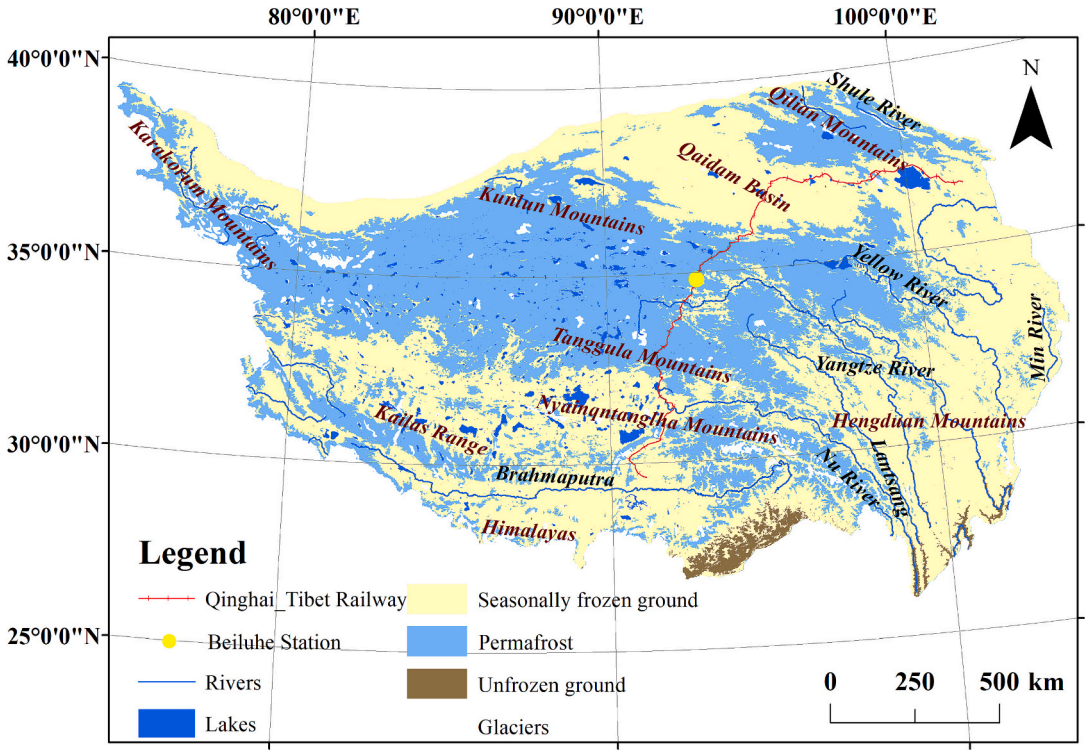

Fig. 1. Geographical location of the Tibetan Plateau, distribution of permafrost on it, and location of the study site. The study site is marked with a yellow dot. Data: permafrost extent is from Zou et al., 2017. (For interpretation of the references to colour in this figure legend, the reader is referred to the web version of this article.)

Table 1
Model parameters used in the simulations.

Parameter	Value	Unit	Source
Air density	0.641	kg m^{-3}	Hou et al., 2020
Albedo of snow-free natural ground surface	0.24	–	You et al., 2017
Albedo of snow-free shoulder surface	0.32	–	Zhang et al., 2019
Albedo of snow-free filling surface	0.26	–	Tai et al., 2020b
Albedo of snow-free railway center surface	0.28	–	Tai et al., 2020b
Thermal conductivity of mineral soil fraction	2.0	W m^{-1} K^{-1}	Wu et al., 2010
Thermal conductivity of air	0.02	W m^{-1} K^{-1}	Hou et al., 2018
Effective thermal conductivity of crushed rock	0.35	W m^{-1} K^{-1}	Hou et al., 2018
Geothermal heat flux	0.072	W m^{-2}	Wu et al., 2010
Volumetric heat capacity of crushed rock	1.006 × 10^6	J K^{-1} m^{-3}	Hou et al., 2018
Root depth in natural ground tile	0.1	m	You et al., 2017
Embankment height above ground	3.7	m	Wu et al., 2020b
Crushed-rock thickness at the centerline	0.4	m	Hou et al., 2018
Width of crushed rock on shady slope	0.8	m	Luo et al., 2018
Width of crushed rock on sunny slope	1.6	m	Luo et al., 2018

crushed rock revetment embankment (CRRE) for reducing the impact of climate change on the embankment and the permafrost beneath the railway. The CRRE is 4.3 m high and 7.2 m wide. The ballast layer is 0.4 m thick and consists of crushed rock with an average particle size of less than 0.1 m (Li et al., 2009). The embankment filling, with a width of 3.7 m above the surface and assumed to be 0.2 m below, is composed of sandy gravel (Tai et al., 2020b; Hou et al., 2020). The width of the crushed rock layer on the embankment slope is 0.8 m on the shady slope and 1.6 m on the sunny slope (Niu et al., 2015), and the particle size ranges from 0.2 to 0.3 m (Cheng et al., 2008). Fig. 2 illustrates our tiling-based model representation of the railway embankment and adjacent natural ground.

2.3.2. Simulation setting

We used anomaly-corrected forcing data from the China Meteorological Forcing Dataset (He et al., 2020) to drive our model based on climatic conditions prevailing at Beiluhe. We generated time series of future climate change considering a low (RCP2.6) and high (RCP8.5) emission scenario (see Supplementary Data Text S3 and Fig. S1 for more details). We divided the embankment structure into nine different tiles to represent the whole railway structure: two natural ground tiles (50 m width), two shoulder tiles (5.55 m width), two outer filling tiles (sunny side: 1.6 m width, shady side: 0.8 m width), two inner filling tiles (1.2 m width), and one center tile (4.8 m width) (Fig. 2). The soil profile is described by a vertical grid that reaches a depth of 1000 m. The thickness of the grid cells increases with depth with a minimum grid cell spacing of 0.02 m for the uppermost soil (top five meters), and a maximum spacing of 100 m at the bottom. Our study site is located on warm and ice-rich permafrost. We assumed excess ice in the ground between 2 m to 5 m below the surface based on field survey data in the Beiluhe basin (Yin et al., 2017; Lin et al., 2020). The geothermal heat flux is about 0.072 Wm^{-2}, as estimated from deep borehole data (Wu et al., 2010). The initial temperature profile in 1979 based on borehole data and set as: 0.4 m: 4.5 °C, 3 m: 0 °C, 10 m: -0.7 °C, 20 m: -0.15 °C, 30 m: 0.15 °C, 100 m: 3.25 °C, 1000 m: 35.65 °C (Yi et al., 2018; Zhang et al., 2020). Supplementary Data Table S2 describes the subsurface ground stratigraphy parameters used in CryoGrid3 for the different tiles. Parameter settings (Table 1) were based on observational evidence as well as on model-based evidence. It should be noted that many studies have shown that the ground temperature and active layer depth on the

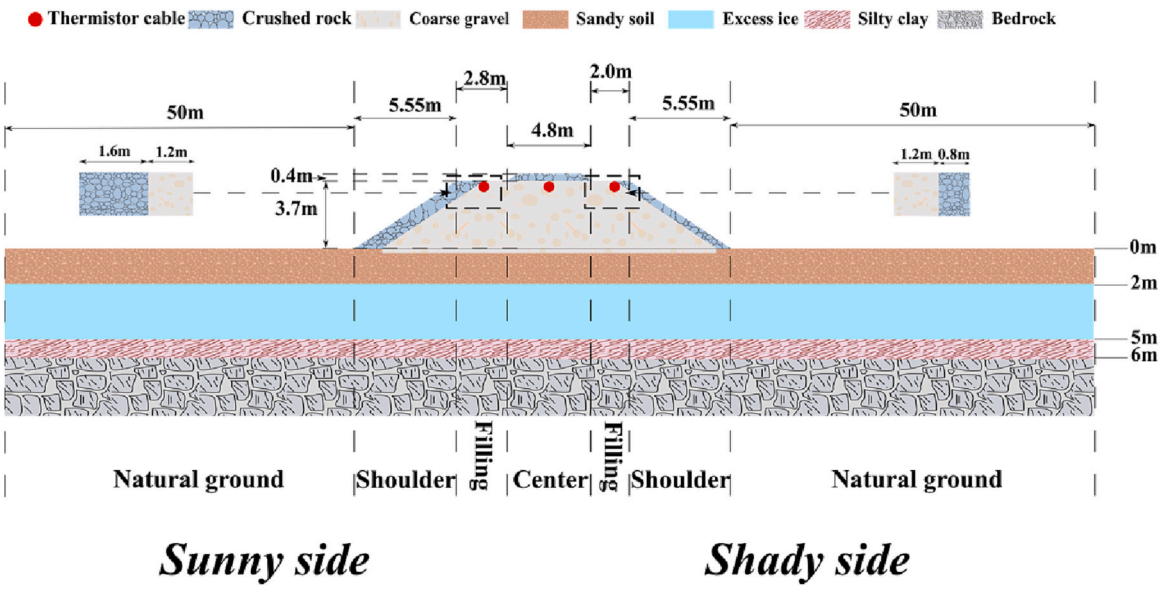

Fig. 2. Schematic diagram of the railway embankment at Beiluhe. Red dots indicate the location of thermistor cables used for validation (the three cables indicated here measured soil temperature at specified depths for the different sections of the railway embankment (sunny filling tile, centerline tile, and shady filling tile). The filling tiles are further subdivided into outer and inner parts (see dashed rectangles). (For interpretation of the references to colour in this figure legend, the reader is referred to the web version of this article.)

sunny slope are significantly greater than on the shaded slope, due to different incoming shortwave radiation. Therefore, we modify the incoming shortwave radiation obtained at the shoulder tile according to the solar elevation angle, azimuth angle, embankment direction, and slope (see Supplementary Data Text S4 and Fig. S2 for details and equations). Moreover, we assumed that snow accumulation at the embankment is not very pronounced given low snow heights in the study regions, and we set maximum snow depths to 0.1 m except for the railway center tile which we assume is snow-free.

3. Results

3.1. Model validation

To validate our model's performance, we compared the modeled and measured mean annual, summer, and winter ground temperatures at three tiles of the railway embankment (centerline, sunny filling tile, and shady filling tile) from 2015 to 2016 (Fig. 3). We further validated the time evolution of ground temperatures at different locations and depths of the subgrade (Fig. 4) and compared modeled and measured ALT (Fig. 5).

A comparison of modeled and observed mean daily ground temperatures showed different magnitudes in annual model-data differences, with biases depending on tile location, but overall good agreement (Fig. 3, left column). The highest deviation was found at 1 m depth on the sunny filling tile of the embankment where the model shows an annual mean cold bias of −0.7 °C. Otherwise, the absolute biases between modeled and measured mean annual values were all less than 0.5 °C. For a more detailed understanding of the model's performance, we compared mean summer (June–July-August) and winter (December–January-February) ground temperature at various soil depths (Fig. 3, center and right columns). The absolute differences between measured and modeled ground temperatures were no more than 1.0 °C in both seasons at all soil depths; the model performed better in summer (the largest bias is below 0.5 °C). To further investigate the temporal evolution of the thermal regimes of the QTR embankment at Beiluhe, we compared the time series of daily average ground temperature (Fig. 4). The results revealed large consistencies between modeled and measured values, with a tendency for simulating colder minimum ground temperatures at 1 m depth on the sunny side as compared to observation data (resulting in a cold bias of approximately −3 °C in March). This bias is not seen in the center or shady filling tiles.

We further compared the modeled and measured ALT (including the natural ground) from 2015 to 2016 (Fig. 5). Observed and modeled ALT were estimated through linear interpolation of vertical profiles of daily ground temperatures (by determining the depth of the 0 °C isotherms). The modeled mean (two years) ALT is 2.17 m (sunny side), 2.34 m (centerline), 2.38 m (shady side), and 2.12 m (natural ground). Measured ALT was larger than the modeled values in all instances. The mean bias between modeled and measured ALT at natural ground tiles was approximately 0.3 m. After adjusting the criterion for the ALT calculation (i.e., ALT determined by +0.1 °C or –0.1 °C isotherm instead of 0 °C isotherm), the upper boundary of modeled ALT was closer to the measured ALT for all infrastructure tiles (Fig. 5, a-c), while the observed ALT for undisturbed natural ground conditions falls within the max-min range of modeled ALT (Fig. 5d). Given our model's tendency for slightly underestimating maximum thaw depths (MTDs) compared to observations, we consider our simulated timing of future railway failure due to permafrost thaw to be rather conservative.

3.2. Evaluation of embankment performance

To illustrate the impact of the QTR on the sub-ground thermal regime, we compared thermal conditions below the railway embankment with conditions inferred below the natural ground away from the railway. Our simulations underline that the crushed-rock embankment structure reveals favorable conditions for the stability of the QTR. The zero degrees isotherm reaches a deeper depth under the natural ground (2.01 m, average value of RCP2.6 and RCP8.5 scenario, for present-day conditions, the year 2020) compared to the sunny and shady shoulder tiles (sunny shoulder: 1.67 m, shady shoulder: 1.22 m, average value of RCP2.6 and RCP8.5 scenario, for present-day conditions, the year 2020) which are covered by crushed rock (Fig. 6 (b) and Fig. 7 (b)). The largest MTDs in the embankment appeared at tiles which were not covered by crushed (sunny and shady inner filling tiles). Due to different amounts of solar radiation and asymmetric crushed rock layer design, simulated ground temperatures at the sunny and shady side reveal significant differences (Fig. 6 and Fig. 7), manifested by a strong "sunny-shady

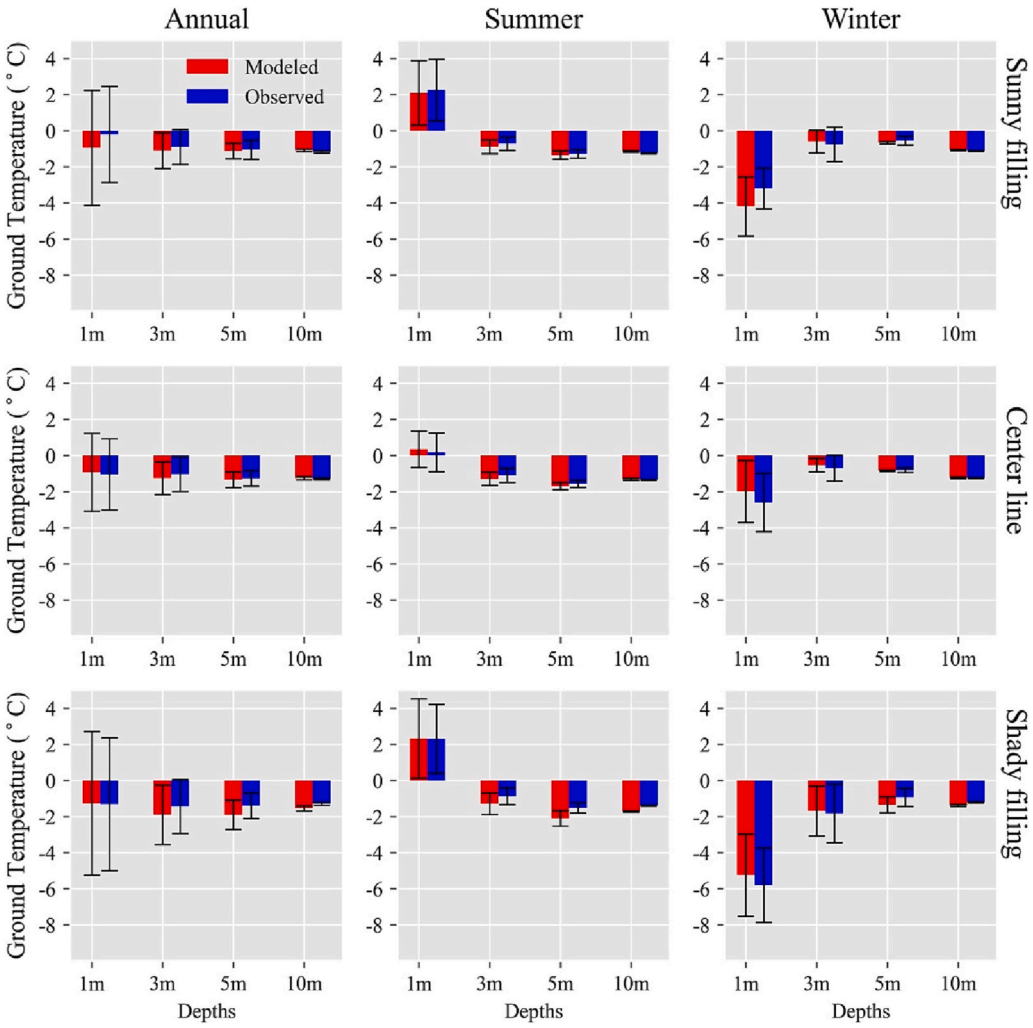

Fig. 3. Average observed and modeled annual ground temperature (left column), average observed and modeled summer ground temperature (June–July-August) (center column), and average observed and modeled winter ground temperature (December–January-February) (right column) plotted against depth at different tiles over a measurement period of 2 years (01-01-2015 to 31-12-2016). The colored bars indicate mean values, the black lines show the standard deviations.

slope effect" with ground temperatures under the sunny side well above ground temperatures under the shady slope. Recent studies have shown that differences in thawing rates below the sunny and the shady sides of an embankment can lead to uneven settlement deformation (Chou et al., 2010; Liu et al., 2016; Tai et al., 2018, 2020b).

Additionally, the artificial permafrost table at all structural tiles of the embankment is still elevated above natural ground conditions. Under current climate conditions, the active layer at sunny slopes almost reaches the embankment base (Fig. 6 (a-b) and Fig. 7 (a-b)). Moderate climate-warming-induced thaw below the embankment at the sunny slope tile seems unavoidable in our simulation, potentially resulting in damage due to thaw settlement. Therefore, protection measures should be considered to maintain the stability of the railway embankment to prolong its service life, such as redesigning the crushed rock revetment (Hou et al., 2020) or increasing the sunny slope albedo (Qin et al., 2016).

3.3. *Future evolution of the railway embankment*

We conducted two experiments to investigate the dynamics of railway embankment thermal regimes to elucidate critical decreases in QTR stability under future climate change. Due to strongly different warming magnitudes under the two considered emission scenarios (with warming up to about 10 °C at Beiluhe towards the end of the century under the RCP8.5 vs. a stabilized climate under the RCP2.6, see Fig. S1) we infer the paths of future permafrost degradation vary considerably for different magnitudes of warming (Fig. 6 (c-h) and Fig. 7 (c-h)). Our simulations suggest that the railway embankment at our considered Beiluhe site might not suffer from subsidence and ground consolidation if the climate is stabilized at the year 2020 levels: thaw depths below the different embankment structure tiles do not further deepen under the RCP2.6, and rather show a slight decrease towards the end of the century (Fig. 6 (c-h)). Yet we emphasize that this conclusion depends on the choice of our used climate model (GFDL-ESM2G) for our analyses. Other climate models (such as MIROC-ESM-CHEM, IPSL-CM5A-LR, and MRI-CGCM3) suggest slight warming trends beyond 2020 over the TP under the RCP2.6 scenario (Su et al., 2013) and therefore could indicate stability of the QTR at Beiluhe even under a low emission scenario as only a little additional warming and thaw depth increase could be enough to trigger ground destabilization under the embankment base.

In contrast, under the strong warming case (RCP8.5), the current crushed rock layer would not be sufficient to protect the structure from failure due to permafrost thaw below the embankment base (Fig. 7 (c-h)). The destabilization of the railway will spread from the sunny side to the shady side. Our modeled thaw front under the sunny slope (Fig. 8e) reaches depths persistently below the embankment base after 2030, while the rest of the embankment might destabilize under further warming after 2040 (Fig. 7 (c-h) and Fig. 8, red dots).

To investigate the temporal dynamics of MTDs and their

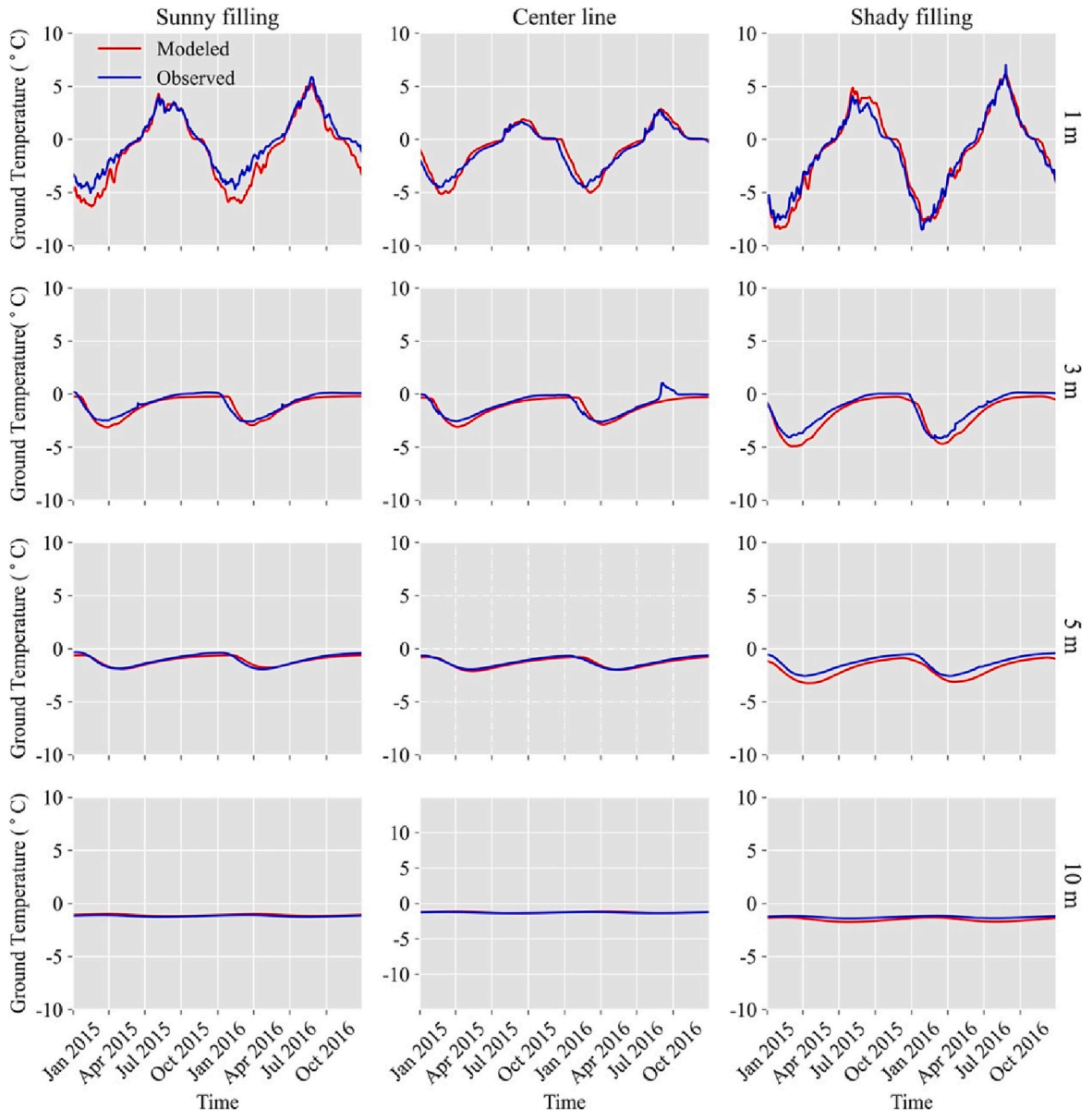

Fig. 4. Time series of modeled (red) and measured (blue) average daily ground temperature at different depths (1, 3, 5, and 10 m) for different embankment tiles (sunny filling, centerline, and shady filling) during the observed period (01-01-2015 to 31-12-2016). (For interpretation of the references to colour in this figure legend, the reader is referred to the web version of this article.)

consequences on the stability of QTR under future climate change, we analyzed the time evolution of MTDs among the different structural tiles. We would like to point out that, in our study, the time at which MTDs begin to persistently penetrate the embankment base is regarded as the start of destabilization of the railway subgrade (from this time onwards, the permafrost table would remain below the embankment base); ultimate embankment destabilization occurs later when the melting of excess ice deeper in the ground will cause subsidence of the embankment structure. MTDs show slight year-to-year variation under low emission pathways, but no discernible trends in the 21st century (Fig. 8, blue dots). The thaw front under the snow-free railway center is higher than that under the other embankment tiles. Subject to strong solar input, the MTDs below the sunny filling tile are deeper than that below the shady filling tile despite a thicker crushed-rock protective layer. The excess ice layer at 2 m depth is not affected by thaw under the RCP2.6 scenario. This suggests, at least when considering the factors accounted for in our model setting, that under stabilizing climate conditions at the year 2020 levels, the QTR might maintain safe operation until the end of the century. The railway embankment will strongly destabilize under extensive warming and settlement of the subgrade will inevitably occur (Fig. 8, red dots) when the thaw front reaches the ice-rich ground. Thaw-induced weakening of the embankment is first inferred at the sunny shoulder in 2031, while the successive thaw of the ground below the base of further embankment tiles might occur more than a decade later. The shady shoulder might resist extensive thaw beyond mid-century but is likely to suffer from mechanical stresses (which we do not simulate) well before ultimate subsidence. Ultimate embankment failure will be triggered by ground subsidence after excess ice melt. In our simulations, this first occurs around mid-century at the sunny shoulder (Fig. 8e, dotted black line), while for the shady shoulder, this might occur about three decades later (Fig. 8f). After full excess ice melt, the ground has subsided by about 0.8 m.

In addition, the lateral asymmetry of the embankment thermal regime would be amplified under a rapid warming trend. The time until MTDs reach the embankment base under the sunny shoulder or occur settlement is significantly less than that under the shady shoulder.

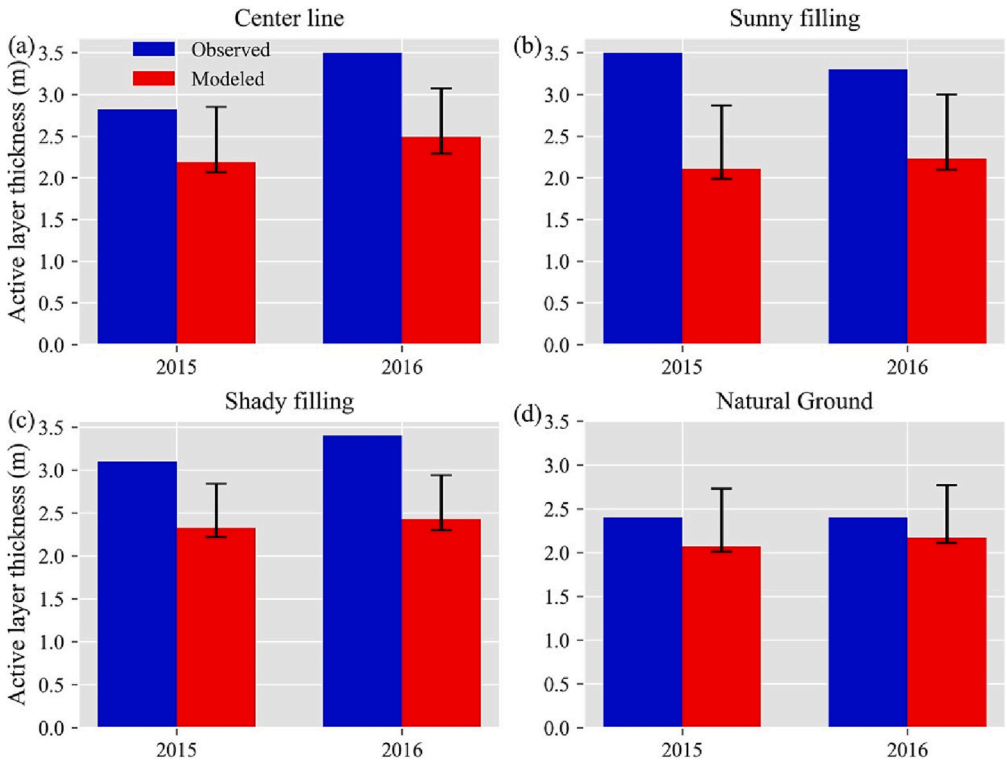

Fig. 5. Measured (blue) and modeled (red) active layer thickness (m) at different railway section tiles (centerline, sunny filling, shady filling, and natural ground) in the years 2015 and 2016. The vertical black lines show the modeled active layer thickness (m) when considering the uncertainty of ±0.1 °C in simulated soil temperature for the 0° isotherm. (For interpretation of the references to colour in this figure legend, the reader is referred to the web version of this article.)

Considering long-term permafrost evolution under climate change, our simulations suggest that under the RCP8.5 climate warming, there is a strong shallowing trend of permafrost thickness at Beiluhe by the end of this century, with potential complete permafrost disappearance in the 22nd century. Further, we analyzed the rate of thaw evolving under the RCP8.5 for all tiles. Our results reveal that thawing rates could be divided into two phases: first, MTDs increase slowly with the mean thaw rate being 5 cm/year. Once critical warming of the ground has been reached, we simulate rapid thaw depth increase with the mean thaw rates between 15 cm to 23 cm per year, occurring between 2040 and 2070 depending on the embankment tile.

4. Discussion

4.1. Comparison with previous modeling studies of the Qinghai-Tibet Railway

This study aims to provide important insights into the stability of the QTR embankment under current and future climate conditions using a physically-based land surface permafrost model driven by localized climate input data. Our modeling results for an embankment section of the QTR at Beiluhe indicate that, under current climate conditions, the sunny-shady slope effect has resulted in a strong asymmetry of the embankment tile thermal regimes. This characteristic of sub-ground temperature distribution agrees with observational analysis (Tai et al., 2020b) and simulation results from geotechnical modeling (Zhang et al., 2011) for the QTR. Under conditions of future intense climate warming, traditional embankment designs (without protection measures) are likely to fail to provide subgrade stability (Lai, 2003; Li et al., 2009; Tang et al., 2021). Modeling studies suggest that all railway crushed-rock embankment subgrades on the TP can provide safe operating conditions for 20 years after embankment construction (around 2025) (Chen et al., 2018; Hou et al., 2018; Tai et al., 2020b), which is consistent with the results of our vulnerability simulations (RCP8.5) (Fig. 7 (c-h) and Fig. 8, red dots). Our modeling results also indicate that CRRE would likely ensure the integrity of railway embankments in the Beiluhe basin until 2030 even under extensive warming. In the 30th year after railway operation (around 2035), the cooling performance of the CRRE will be significantly reduced, as evidenced by the MTDs at the sunny shoulder are projected to extend below the embankment base by this time, indicating that the railway subgrade has become destabilized (Fig. 7 (c-h) and Fig. 8, red dots). If the service period is extended to 50 years (around 2055), there are significant differences in the effectiveness of the protection among crushed-rock embankments under severe climate warming. For example, our study indicates that, under the RCP8.5 scenario, CRRE is not sufficient to maintain the safe operation of the QTR, especially on the sunny side. At mid-century, the upper boundary of permafrost will remain above the embankment base only at the shady shoulder. Our estimated MTDs at the centerline (6.25 m) in the 50th service year is consistent with the values reported in previous studies (6.4 m) based on geotechnical modeling to simulate the thermal regime of CRRE (Hou et al., 2020). Our modeling results suggest that the CRRE may remain stable until 2030, but redesign and reinforcement are essential for a safe long-term operation of the railway under climate warming. Our analyses of thaw propagation in natural ground indicate that MTDs will fluctuate around 2 m underground until the end of the century under the RCP2.6 scenario, while under the RCP8.5 scenario, the MTDs will reach to a depth of around 15 m (Fig. 8a), close to the lower boundary of permafrost at our research site (20 m). For the Beiluhe area, the GIPL model indicates that the average ALT will range from 2.5 to 3 m under comparatively small surface air warming trends (0.15 °C/decade) by the third quarter of the 21st century (2046–2075); this is larger than our modeled results (average ALT is 1.83 m during 2046 to 2075). Under the severe warming scenario (RCP8.5), our estimated average ALT will reach 4.52 m (from 2046 to 2075) which is deeper than the results from Luo et al. (2019) (their average ALT is from 3.0 to 3.5 m). This difference could be explained by the difference in considered surface air warming trends (this study: 0.9 °C/decade, Luo

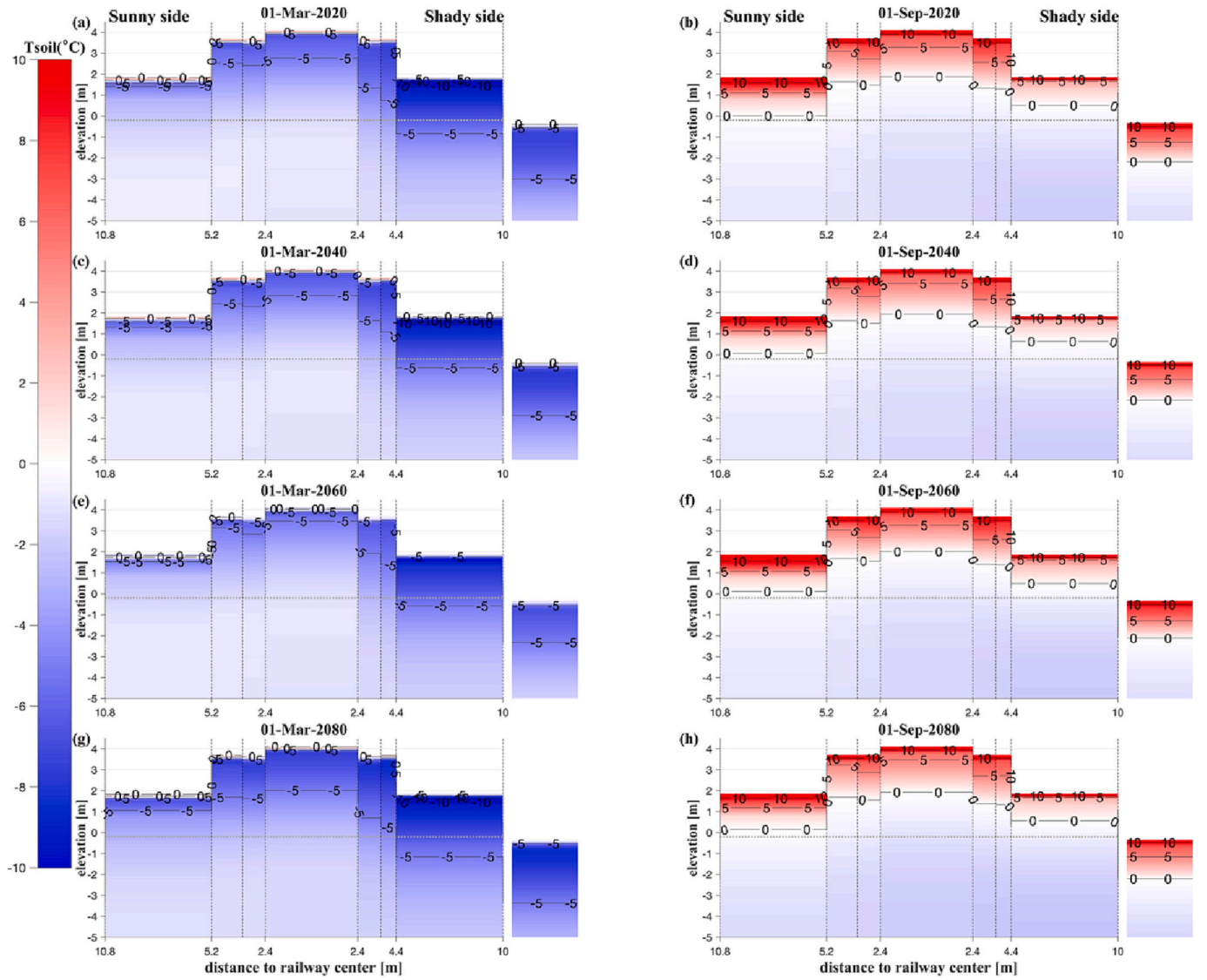

Fig. 6. Modeled ground temperatures in the crushed-rock railway embankment on 1 March (a, c, e, g) and 1 September (b, d, f, h) under the RCP2.6 scenario for current (a-b) and future conditions (c-h). The separate right columns indicate the temperature profile of the outermost tile (natural ground). Dashed vertical lines indicate the separation into the structural tiles. Dotted horizontal lines represent the embankment base.

et al. (2019): 0.65 °C/decade).

4.2. Model limitation

Our model simulations are able to realistically capture the thermal ground state of the embankment structure at our considered Beiluhe site under present-day conditions (see Section 3.2). In our study, we underestimate uncertainty in future climate change by not considering the full spread of model uncertainty as displayed by CMIP models. Furthermore, the latest generation earth system models (CMIP6) project higher temperature changes and accelerated warming trends relative to CMIP5 models (Zhou et al., 2022), indicating that the QTR embankment may face earlier instability issues compared to our analyses based on CMIP5 models. When evaluating the concrete risk of failure for the QTR at Beiluhe we might have missed certain factors of potential importance to embankment structure stability in our model setup. It has been discussed that the combined effect of aeolian sand deposition and climate change will further accelerate permafrost degradation (Yu et al., 2016; Chen et al., 2018) but we do not consider the aeolian sand deposition effect which can negatively affect the cooling mechanism of the crushed-rock embankment. We, therefore, consider our results on the timing of future permafrost degradation at Beiluhe to be rather conservative. Further, we do not explicitly model convective heat transport within the crushed rock layers but rather tune the thermal properties of the embankment material to mimic the effect of convective cooling and to capture realistic thermal sub-ground conditions. We also want to point out that our assumption of the depth and thickness of the excess ice layer has a significant impact on the timing of railway embankment subsidence. We based our assumption on field data from ground ice measurements in the Beiluhe basin, but site-specific measurements would be needed for a tailored risk assessment of the QTR at Beiluhe. In this study, we focus on modeling the thermal regime of the embankment and assessing the impact of climate warming on railway stability; we do not consider the influence of mechanical stresses on embankment stability. This will be an issue for strongly asymmetrical warming, with impacts on stability being further aggravated if mechanical stresses from traffic load are also considered. Therefore, using state-of-art model is required to elucidate the full spectrum of factors impacting embankment stability.

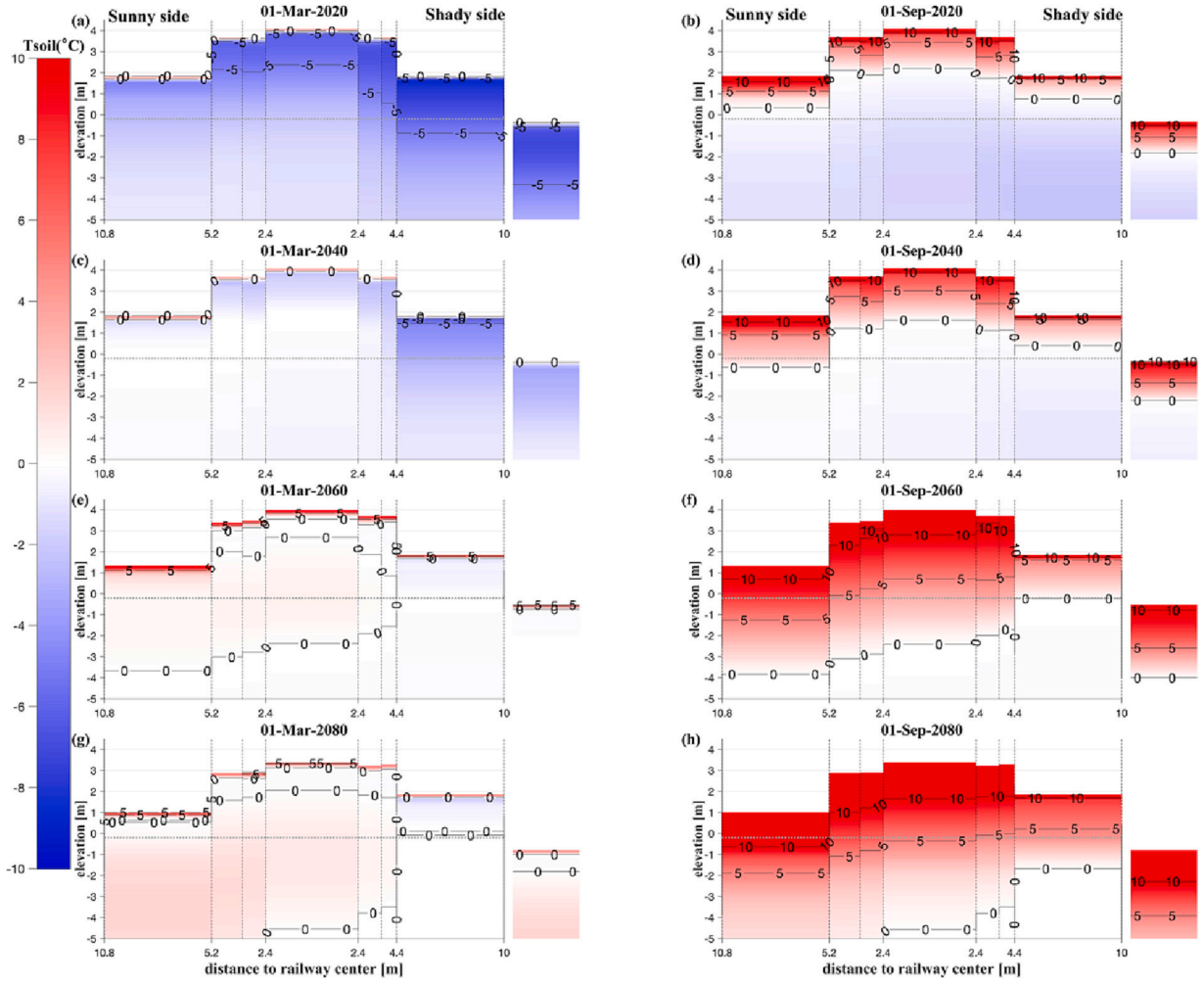

Fig. 7. Same as Fig. 6, but under the RCP8.5 scenario.

5. Conclusion

In this study, we apply a laterally coupled version of the one-dimensional land surface model CryoGrid3 which enables us to represent different parts of a railway embankment on the Tibetan Plateau. We investigate the impact of climate warming on infrastructure threatened by ground subsidence from excess ice melt. By comparing our model simulations with observational data, we show that our model is able to reflect the temporal thaw dynamics in the ground at different railway tiles. Using this model, we conducted several experiments to quantify the thermal regimes of the railway embankment under both current climate and future conditions. Our main conclusions are as follows.

1. Crushed rock can efficiently protect the underground permafrost from heat penetration resulting in shallower maximum thaw depths as compared to thaw depths under natural ground.
2. Our simulations suggest that the artificial permafrost table at our considered site at Beiluhe for the sunny side of the embankment shoulder is already close to the embankment base under present-day climate conditions. This points to a high risk of future failure under climate warming.
3. Our model analyses suggest that the railway embankment at Beiluhe will likely be stable if climate stabilizes at present-day (2020) conditions, otherwise asymmetrical vertical temperature gradients between the sunny and shady shoulders might lead to stability issues.
4. Future permafrost warming will lead to ultimate infrastructure failure due to ground subsidence when the thaw depth reaches the ice-rich ground. Our simulations under the RCP8.5 scenario point to the risk of severe destabilization starting in the 2030s and full failure due to the settlement of the embankment structure occurring around mid-century under unabated climate warming.

In summary, our study provides a computationally efficient approach for modeling the thermal regime of infrastructure on the TP in response to 21st-century climate changes. By modeling ground subsidence, we illustrate the risk of infrastructure failure of the QTR at Beiluhe due to infrastructure settlement after excess ice melt. Our modeling results underline the fact that the current protection of the QTR embankment against thaw-induced destabilization might not be sufficient in the future even under moderate rates of temperature increases. Yet we emphasize that concrete risk assessments require additional studies with highly resolved (geo-technical) models which account for the full spectrum of site-specific factors that are important to infrastructure stability.

CRediT authorship contribution statement

Rui Chen: Conceptualization, Methodology, Validation, Visualization, Formal analysis, Software, Writing – original draft. **Thomas Schneider von Deimling:** Conceptualization, Methodology, Software, Writing – review & editing, Supervision. **Julia Boike:** Writing – review & editing, Supervision. **Qingbai Wu:** Resources. **Moritz Langer:** Writing – review & editing, Supervision, Software, Funding acquisition.

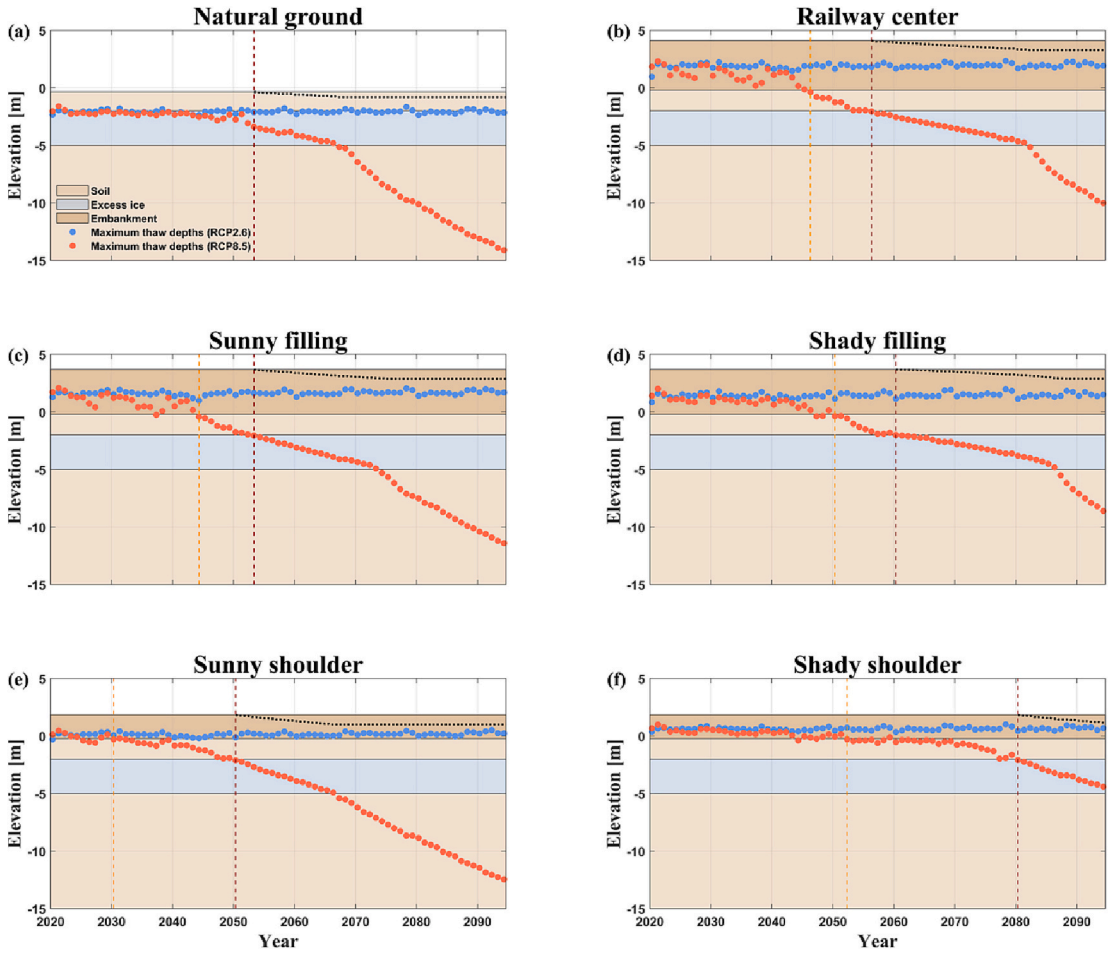

Fig. 8. Temporal evolution of the railway embankment state under climate change. Blue and red dots illustrate the change in maximum thaw depths under natural ground (a) and under different embankment tiles (b-f) for the RCP2.6 and RCP8.5 scenarios. The dotted black line represents the time evolution of the ground surface elevation under subsidence (RCP8.5). Dashed vertical lines represent the stability loss of the embankment under the RCP8.5 warming scenario (orange: the beginning of sub-grade persistent destabilization, dark red: the beginning of subsidence). (For interpretation of the references to colour in this figure legend, the reader is referred to the web version of this article.)

Declaration of Competing Interest

None.

Data availability

The China Meteorological Forcing Dataset used for generating climate forcing timeseries is available at www.data.tpdc.ac.cn. The climate change scenario model runs (GFDL-ESM2G and GFDL-CM3) are available at https://esgf-data.dkrz.de/search/cmip5-dkrz/. The model source code used for the simulations in this work is archived on Zenodo (https://doi.org/10.5281/zenodo.7778477). The observed ground temperature data at Beiluhe (for the adjacent tundra and for the railway embankment) were obtained from the coauthor of this study: Prof. Qingbai Wu (qbwu@lzb.ac.cn).

Acknowledgments

This work was supported by the Federal Ministry of Education and Research (BMBF) of Germany through a grant to Moritz Langer (No. 01LN1709A). Additional support came from the AWI Innovation Funds (Innovation Project IP10200006), and the China Scholarship Council (201904910442).

Appendix A. Supplementary data

Supplementary data to this article can be found online at https://doi.org/10.1016/j.coldregions.2023.103881.

References

Chen, L., Yu, W., Yi, X., Hu, D., Liu, W., 2018. Numerical simulation of heat transfer of the crushed-rock interlayer embankment of Qinghai-Tibet Railway affected by aeolian sand clogging and climate change. Cold Reg. Sci. Technol. 155, 1–10. https://doi.org/10.1016/j.coldregions.2018.07.009.

Chen, R., Li, H., Wang, X., Gou, X., Yang, M., Wan, G., 2022. Surface air temperature changes over the Tibetan Plateau: historical evaluation and future projection based on CMIP6 models. Geosci. Front. 13, 101452 https://doi.org/10.1016/j.gsf.2022.101452.

Cheng, G., Sun, Z., Niu, F., 2008. Application of the roadbed cooling approach in Qinghai–Tibet railway engineering. Cold Reg. Sci. Technol. 53, 241–258. https://doi.org/10.1016/j.coldregions.2007.02.006.

Chou, Y., Sheng, Y., Li, Y., Wei, Z., Zhu, Y., Li, J., 2010. Sunny–shady slope effect on the thermal and deformation stability of the highway embankment in warm permafrost regions. Cold Reg. Sci. Technol. 63, 78–86. https://doi.org/10.1016/j.coldregions.2010.05.001.

Duan, A., Xiao, Z., 2015. Does the climate warming hiatus exist over the Tibetan Plateau? Sci. Rep. 5, 13711. https://doi.org/10.1038/srep13711.

Fortier, R., LeBlanc, A.-M., Yu, W., 2011. Impacts of permafrost degradation on a road embankment at Umiujaq in Nunavik (Quebec), Canada. Can. Geotech. J. 48, 720–740. https://doi.org/10.1139/t10-101.

Guo, L., Xie, Y., Yu, Q., You, Y., Wang, X., Li, X., 2016. Displacements of tower foundations in permafrost regions along the Qinghai–Tibet Power Transmission Line. Cold Reg. Sci. Technol. 121, 187–195. https://doi.org/10.1016/j.coldregions.2015.07.012.

He, J., Yang, K., Tang, W., Lu, H., Qin, J., Chen, Y., Li, X., 2020. The first high-resolution meteorological forcing dataset for land process studies over China. Sci. Data 7, 25. https://doi.org/10.1038/s41597-020-0369-y.

Hjort, J., Streletskiy, D., Doré, G., Wu, Q., Bjella, K., Luoto, M., 2022. Impacts of permafrost degradation on infrastructure. Nat. Rev. Earth Environ. 3, 24–38. https://doi.org/10.1038/s43017-021-00247-8.

Hou, Y., Wu, Q., Dong, J., Luo, J., Zhang, M., Ye, Z., 2018. Numerical simulation of efficient cooling by coupled RR and TCPT on railway embankments in permafrost regions. Appl. Therm. Eng. 133, 351–360. https://doi.org/10.1016/j.applthermaleng.2018.01.070.

Hou, Y., Wu, Q., Wang, K., Ye, Z., 2020. Numerical evaluation for protecting and reinforcing effect of a new designed crushed rock revetment on Qinghai–Tibet Railway. Renew. Energy 156, 645–654. https://doi.org/10.1016/j.renene.2020.04.066.

Kong, X., Doré, G., Calmels, F., 2019. Thermal modeling of heat balance through embankments in permafrost regions. Cold Reg. Sci. Technol. 158, 117–127. https://doi.org/10.1016/j.coldregions.2018.11.013.

Lai, Y., 2003. Cooling effect of ripped-stone embankments on Qing-Tibet railway under climatic warming. Chin. Sci. Bull. 48, 598. https://doi.org/10.1360/03tb9127.

Lai, Y., Wang, Q., Niu, F., Zhang, K., 2004a. Three-dimensional nonlinear analysis for temperature characteristic of ventilated embankment in permafrost regions. Cold Reg. Sci. Technol. 38, 165–184. https://doi.org/10.1016/j.coldregions.2003.10.006.

Lai, Y., Zhang, S., Zhang, L., Xiao, J., 2004b. Adjusting temperature distribution under the south and north slopes of embankment in permafrost regions by the ripped-rock revetment. Cold Reg. Sci. Technol. 39, 67–79. https://doi.org/10.1016/j.coldregions.2004.04.003.

Lai, Y., Zhang, M., Liu, Z., Yu, W., 2006. Numerical analysis for cooling effect of open boundary ripped-rock embankment on Qinghai-Tibetan railway. Sci. China Ser. D 49, 764–772. https://doi.org/10.1007/s11430-006-0764-z.

Langer, M., Westermann, S., Boike, J., Kirillin, G., Grosse, G., Peng, S., Krinner, G., 2016. Rapid degradation of permafrost underneath waterbodies in tundra landscapes—toward a representation of thermokarst in land surface models. J. Geophys. Res. Earth Surf. 121, 2446–2470. https://doi.org/10.1002/2016JF003956.

Li, S., Lai, Y., Zhang, M., Dong, Y., 2009. Study on long-term stability of Qinghai–Tibet Railway embankment. Cold Reg. Sci. Technol. 57, 139–147. https://doi.org/10.1016/j.coldregions.2009.02.003.

Lin, Z., Gao, Z., Fan, X., Niu, F., Luo, J., Yin, G., Liu, M., 2020. Factors controlling near surface ground-ice characteristics in a region of warm permafrost, Beiluhe Basin, Qinghai-Tibet Plateau. Geoderma 376, 114540. https://doi.org/10.1016/j.geoderma.2020.114540.

Liu, H., Niu, F., Niu, Y., Xu, J., Wang, T., 2016. Effect of structures and sunny–shady slopes on thermal characteristics of subgrade along the Harbin–Dalian Passenger Dedicated Line in Northeast China. Cold Reg. Sci. Technol. 123, 14–21. https://doi.org/10.1016/j.coldregions.2015.11.007.

Luo, J., Niu, F., Liu, M., Lin, Z., Yin, G., 2018. Field experimental study on long-term cooling and deformation characteristics of crushed-rock revetment embankment at the Qinghai–Tibet Railway. Appl. Therm. Eng. 139, 256–263. https://doi.org/10.1016/j.applthermaleng.2018.04.138.

Luo, J., Yin, G., Niu, F., Lin, Z., Liu, M., 2019. High spatial resolution modeling of climate change impacts on permafrost thermal conditions for the Beiluhe Basin, Qinghai-Tibet Plateau. Remote Sens. 11, 1294. https://doi.org/10.3390/rs11111294.

Ma, W., Feng, G., Wu, Q., Wu, J., 2008. Analyses of temperature fields under the embankment with crushed-rock structures along the Qinghai–Tibet Railway. Cold Reg. Sci. Technol. 53, 259–270. https://doi.org/10.1016/j.coldregions.2007.08.001.

Ma, W., Wen, Z., Sheng, Y., Wu, Q., Wang, D., Feng, W., 2012. Remedying embankment thaw settlement in a warm permafrost region with thermosyphons and crushed rock revetment. Can. Geotech. J. 49, 1005–1014. https://doi.org/10.1139/t2012-058.

Martin, L.C.P., Nitzbon, J., Scheer, J., Aas, K.S., Eiken, T., Langer, M., Filhol, S., Etzelmüller, B., Westermann, S., 2021. Lateral thermokarst patterns in permafrost peat plateaus in northern Norway. Cryosphere 15, 3423–3442. https://doi.org/10.5194/tc-15-3423-2021.

Mu, Y., Ma, W., Liu, Y., Sun, Z., 2010. Monitoring investigation on thermal stability of air-convection crushed-rock embankment. Cold Reg. Sci. Technol. 62, 160–172. https://doi.org/10.1016/j.coldregions.2010.03.007.

Nitzbon, J., Langer, M., Westermann, S., Martin, L., Aas, K.S., Boike, J., 2019. Pathways of ice-wedge degradation in polygonal tundra under different hydrological conditions. Cryosphere 13, 1089–1123. https://doi.org/10.5194/tc-13-1089-2019.

Nitzbon, J., Westermann, S., Langer, M., Martin, L.C.P., Strauss, J., Laboor, S., Boike, J., 2020. Fast response of cold ice-rich permafrost in Northeast Siberia to a warming climate. Nat. Commun. 11, 2201. https://doi.org/10.1038/s41467-020-15725-8.

Nitzbon, J., Langer, M., Martin, L.C.P., Westermann, S., Schneider von Deimling, T., Boike, J., 2021. Effects of multi-scale heterogeneity on the simulated evolution of ice-rich permafrost lowlands under a warming climate. Cryosphere 15, 1399–1422. https://doi.org/10.5194/tc-15-1399-2021.

Niu, F., Liu, M., Cheng, G., Lin, Z., Luo, J., Yin, G., 2015. Long-term thermal regimes of the Qinghai-Tibet Railway embankments in plateau permafrost regions. Sci. China Earth Sci. 58, 1669–1676. https://doi.org/10.1007/s11430-015-5063-0.

Peng, H., Ma, W., Mu, Y., Jin, L., 2015. Impact of permafrost degradation on embankment deformation of Qinghai-Tibet Highway in permafrost regions. J. Cent. South Univ. 22, 1079–1086. https://doi.org/10.1007/s11771-015-2619-2.

Qin, Y., Zhang, J., Li, G., Qu, G., 2010. Settlement characteristics of unprotected embankment along the Qinghai–Tibet Railway. Cold Reg. Sci. Technol. 60, 84–91. https://doi.org/10.1016/j.coldregions.2009.08.002.

Qin, Y., Liang, J., Luo, Z., Tan, K., Zhu, Z., 2016. Increasing the southern side-slope albedo remedies thermal asymmetry of cold-region roadway embankments. Cold Reg. Sci. Technol. 123, 115–120. https://doi.org/10.1016/j.coldregions.2015.12.006.

Ran, Y., Li, X., Cheng, G., Nan, Z., Che, J., Sheng, Y., Wu, Q., Jin, H., Luo, D., Tang, Z., Wu, X., 2021. Mapping the permafrost stability on the Tibetan Plateau for 2005–2015. Sci. China Earth Sci. 64, 62–79. https://doi.org/10.1007/s11430-020-9685-3.

Schneider von Deimling, T., Lee, H., Ingeman-Nielsen, T., Westermann, S., Romanovsky, V., Lamoureux, S., Walker, D.A., Chadburn, S., Trochim, E., Cai, L., Nitzbon, J., Jacobi, S., Langer, M., 2021. Consequences of permafrost degradation for Arctic infrastructure – bridging the model gap between regional and engineering scales. Cryosphere 15, 2451–2471. https://doi.org/10.5194/tc-15-2451-2021.

Stuenzi, S.M., Boike, J., Cable, W., Herzschuh, U., Kruse, S., Pestryakova, L.A., Schneider von Deimling, T., Westermann, S., Zakharov, E.S., Langer, M., 2021. Variability of the surface energy balance in permafrost-underlain boreal forest. Biogeosciences 18, 343–365. https://doi.org/10.5194/bg-18-343-2021.

Su, F., Duan, X., Chen, D., Hao, Z., Cuo, L., 2013. Evaluation of the global climate models in the CMIP5 over the Tibetan Plateau. J. Clim. 26, 3187–3208. https://doi.org/10.1175/JCLI-D-12-00321.1.

Sun, B., Xu, X., Lai, Y., Fang, M., 2005. Evaluation of fractured rock layer heights in ballast railway embankment based on cooling effect of natural convection in cold regions. Cold Reg. Sci. Technol. 42, 120–144. https://doi.org/10.1016/j.coldregions.2005.01.001.

Sun, B., Yang, L., Liu, Q., Wang, W., Xu, X., 2009. Numerical analysis for critical thickness of crushed rock revetment layer on Qinghai–Tibet Railway. Cold Reg. Sci. Technol. 57, 131–138. https://doi.org/10.1016/j.coldregions.2009.02.005.

Tai, B., Liu, Jiankun, Yue, Z., Liu, Jingyu, Tian, Y., Wang, T., 2018. Effect of sunny-shady slopes and strike on thermal regime of subgrade along a high-speed railway in cold regions, China. Eng. Geol. 232, 182–191. https://doi.org/10.1016/j.enggeo.2017.09.002.

Tai, B., Wu, Q., Zhang, Z., Xu, X., 2020a. Cooling performance and deformation behavior of crushed-rock embankments on the Qinghai-Tibet Railway in permafrost regions. Eng. Geol. 265, 105453 https://doi.org/10.1016/j.enggeo.2019.105453.

Tai, B., Wu, Q., Zhang, Z., Xu, X., 2020b. Study on thermal performance of novel asymmetric crushed-rock-based embankment on the Qinghai-Tibet Railway in permafrost region. Int. J. Therm. Sci. 152, 106333 https://doi.org/10.1016/j.ijthermalsci.2020.106333.

Tang, C., Zhu, Z., Luo, F., He, Z., Zou, Z., Guo, Z., 2021. Deformation behaviour and influence mechanism of thaw consolidation of embankments on the Qinghai-Tibet Railway in permafrost regions. Transp. Geotech. 28, 100513 https://doi.org/10.1016/j.trgeo.2021.100513.

Tian, Y., Yang, Z.J., Tai, B., Li, Y., Shen, Y., 2019. Damage and mitigation of railway embankment drainage trench in warm permafrost: a case study. Eng. Geol. 261, 105276 https://doi.org/10.1016/j.enggeo.2019.105276.

Wang, X., Pang, G., Yang, M., Zhao, G., 2017. Evaluation of climate on the Tibetan Plateau using ERA-Interim reanalysis and gridded observations during the period 1979–2012. Quat. Int. 444, 76–86. https://doi.org/10.1016/j.quaint.2016.12.041. Third Pole: The Last 20,000 Years - Part 2.

Wang, X., Ran, Y., Pang, G., Chen, D., Su, B., Chen, R., Li, X., Chen, H.W., Yang, M., Gou, X., Jorgenson, M.T., Aalto, J., Li, R., Peng, X., Wu, T., Clow, G.D., Wan, G., Wu, X., Luo, D., 2022. Contrasting characteristics, changes, and linkages of permafrost between the Arctic and the Third Pole. Earth-Sci. Rev. 230, 104042 https://doi.org/10.1016/j.earscirev.2022.104042.

Westermann, S., Langer, M., Boike, J., Heikenfeld, M., Peter, M., Etzelmüller, B., Krinner, G., 2016. Simulating the thermal regime and thaw processes of ice-rich permafrost ground with the land-surface model CryoGrid 3. Geosci. Model Dev. 9, 523–546. https://doi.org/10.5194/gmd-9-523-2016.

Wu, Q., Yongzhi, L., Jianming, Z., Changjiang, T., 2002. A review of recent frozen soil engineering in permafrost regions along Qinghai-Tibet Highway, China. Permafr. Periglac. Process. 13, 199–205. https://doi.org/10.1002/ppp.420.

Wu, Q., Zhang, T., Liu, Y., 2010. Permafrost temperatures and thickness on the Qinghai-Tibet Plateau. Glob. Planet. Chang. 72, 32–38. https://doi.org/10.1016/j.gloplacha.2010.03.001.

Wu, Q., Niu, F., Ma, W., Liu, Y., 2014. The effect of permafrost changes on embankment stability along the Qinghai–Xizang Railway. Environ. Earth Sci. 71, 3321–3328. https://doi.org/10.1007/s12665-013-2718-z.

Wu, Q., Zhang, Z., Gao, S., Ma, W., 2016. Thermal impacts of engineering activities and vegetation layer on permafrostin different alpine ecosystems of the Qinghai–Tibet Plateau, China. Cryosphere 10, 1695–1706. https://doi.org/10.5194/tc-10-1695-2016.

Wu, Q., Sheng, Y., Yu, Q., Chen, J., Ma, W., 2020a. Engineering in the rugged permafrost terrain on the roof of the world under a warming climate. Permafr. Periglac. Process. 31, 417–428. https://doi.org/10.1002/ppp.2059.

Wu, Q., Zhao, H., Zhang, Z., Chen, J., Liu, Y., 2020b. Long-term role of cooling the underlying permafrost of the crushed rock structure embankment along the Qinghai–Xizang railway. Permafr. Periglac. Process. 31, 172–183. https://doi.org/10.1002/ppp.2027.

Xu, X., Wu, Q., 2021. Active layer thickness variation on the Qinghai-Tibetan Plateau: historical and projected trends. J. Geophys. Res.-Atmos. 126 https://doi.org/10.1029/2021JD034841 e2021JD034841.

Yan, Y., You, Q., Wu, F., Pepin, N., Kang, S., 2020. Surface mean temperature from the observational stations and multiple reanalyses over the Tibetan Plateau. Clim. Dyn. 55, 2405–2419. https://doi.org/10.1007/s00382-020-05386-0.

Yang, J., Zhong, F., Xu, X., Wu, Q.B., 2018. Quantitative evaluation of the impact of the Qinghai-Tibet Railway on the development of various economic sectors in Tibet. J. Glaciol. Geocryol. 40, 1047–1055 (in Chinese). https://doi.org/10.7522/j.issn.1000-0240.2018.0313 (in Chinese).

Yang, M., Wang, X., Pang, G., Wan, G., Liu, Z., 2019. The Tibetan Plateau cryosphere: observations and model simulations for current status and recent changes. Earth-Sci. Rev. 190, 353–369. https://doi.org/10.1016/j.earscirev.2018.12.018.

Yi, S., He, Y., Guo, X., Chen, J., Wu, Q., Qin, Y., Ding, Y., 2018. The physical properties of coarse-fragment soils and their effects on permafrost dynamics: a case study on the central Qinghai–Tibetan Plateau. Cryosphere 12, 3067–3083. https://doi.org/10.5194/tc-12-3067-2018.

Yin, G., Niu, F., Lin, Z., Luo, J., Liu, M., 2017. Effects of local factors and climate on permafrost conditions and distribution in Beiluhe basin, Qinghai-Tibet Plateau, China. Sci. Total Environ. 581–582, 472–485. https://doi.org/10.1016/j.scitotenv.2016.12.155.

Yin, G.-A., Niu, F.-J., Lin, Z.-J., Luo, J., Liu, M.-H., 2021. Data-driven spatiotemporal projections of shallow permafrost based on CMIP6 across the Qinghai–Tibet Plateau at 1 km2 scale. Adv. Clim. Chang. Res. 12, 814–827. https://doi.org/10.1016/j.accre.2021.08.009.

You, Q., Xue, X., Peng, F., Dong, S., Gao, Y., 2017. Surface water and heat exchange comparison between alpine meadow and bare land in a permafrost region of the Tibetan Plateau. Agric. For. Meteorol. 232, 48–65. https://doi.org/10.1016/j.agrformet.2016.08.004.

Yu, W., Liu, W., Chen, L., Yi, X., Han, F., Hu, D., 2016. Evaluation of cooling effects of crushed rock under sand-filling and climate warming scenarios on the Tibet Plateau. Appl. Therm. Eng. 92, 130–136. https://doi.org/10.1016/j.applthermaleng.2015.09.030.

Zhang, M., Lai, Y., Liu, Z., Gao, Z., 2005. Nonlinear analysis for the cooling effect of Qinghai-Tibetan railway embankment with different structures in permafrost regions. Cold Reg. Sci. Technol. 42, 237–249. https://doi.org/10.1016/j.coldregions.2005.02.003.

Zhang, M., Lai, Y., Yu, W., Huang, Z., 2007. Experimental study on influence of particle size on cooling effect of crushed-rock layer under closed and open tops. Cold Reg. Sci. Technol. 48, 232–238. https://doi.org/10.1016/j.coldregions.2006.12.003.

Zhang, M., Cheng, G., Li, S., 2009. Numerical study on the influence of geometrical parameters on natural convection cooling effect of the crushed-rock revetment. Sci. China Ser. E Technol. Sci. 52, 539–545. https://doi.org/10.1007/s11431-008-0329-9.

Zhang, M., Wu, Z., Wang, J., Lai, Y., You, Z., 2019. Experimental and theoretical studies on the solar reflectance of crushed-rock layers. Cold Reg. Sci. Technol. 159, 13–19. https://doi.org/10.1016/j.coldregions.2018.10.012.

Zhang, K., Li, D., Niu, F., Mu, Y., 2011. Cooling effects study on ventilated embankments under the influence of the temperature differences between the sunny slopes and the shady slopes. Cold Reg. Sci. Technol. 65, 226–233. https://doi.org/10.1016/j.coldregions.2010.08.005.

Zhang, Z., Wu, Q., Jiang, G., Gao, S., Chen, J., Liu, Y., 2020. Changes in the permafrost temperatures from 2003 to 2015 in the Qinghai-Tibet Plateau. Cold Reg. Sci. Technol. 169, 102904 https://doi.org/10.1016/j.coldregions.2019.102904.

Zhao, H., Wu, Q., Zhang, Z., 2019. Long-term cooling effect of the crushed rock structure embankments of the Qinghai–Tibet Railway. Cold Reg. Sci. Technol. 160, 21–30. https://doi.org/10.1016/j.coldregions.2019.01.006.

Zhou, M., Yu, Z., Gu, H., Ju, Q., Gao, Y., Wen, L., Huang, T., Wang, W., 2022. Evaluation and projections of surface air temperature over the Tibetan Plateau from CMIP6 and CMIP5: warming trend and uncertainty. Clim. Dyn. https://doi.org/10.1007/s00382-022-06518-4.

Zou, D., Zhao, L., Sheng, Y., Chen, J., Hu, G., Wu, T., Wu, J., Xie, C., Wu, X., Pang, Q., Wang, W., Du, E., Li, W., Liu, G., Li, J., Qin, Y., Qiao, Y., Wang, Z., Shi, J., Cheng, G., 2017. A new map of permafrost distribution on the Tibetan Plateau. Cryosphere 11, 2527–2542. https://doi.org/10.5194/tc-11-2527-2017.